Journal of Analytical Atomic Spectroscopy

Supporting Information for

A Prospective Microwave Plasma Source for In Situ Spaceflight Applications

B. Farcy[a], R. Arevalo Jr.[a*], M. Taghiouskoui[b], W. McDonough[a,c], M. Benna[d], W. Brinckerhoff[d]

[a]Department of Geology, University of Maryland, College Park MD, 20742, USA

[b]Trace Matters Scientific, Somerville MA, USA, 02143

[c]Department of Earth Sciences and Research Center for Neutrino Science, Tohoku University, Sendai, Miyagi, 980-8578, Japan

[d]NASA Goddard Space Flight Center, Greenbelt MD, USA, 20771

Contents of this file

Plasma Characterization by Optical Emission Spectroscopy

In addition to plasma analysis using a Langmuir probe, electron density (N_e) and temperature (T_e) can also be measured in a plasma spectroscopically. We injected analytes into a commercial plasma and measured relevant physical parameters (T_e and N_e) using an inductively coupled plasma optical emission spectroscopy (Shimadzu 9800 ICPOES).

Three samples of single element standard solutions with different first ionization potentials were used to compare the predicted Saha ionization efficiency with directly measured ionization efficiency. We used 10 µg/ml solutions of La (5.5 eV, first ionization potential), Mg (7.6 eV), and Zn (9.4 eV) dissolved in HNO_3. The emission spectra of both ionized and neutral species were determined. Constants and statistical parameters for each emission were taken from the NIST atomic spectroscopy database (Kramida, Ralchenko and Reader, 2018).

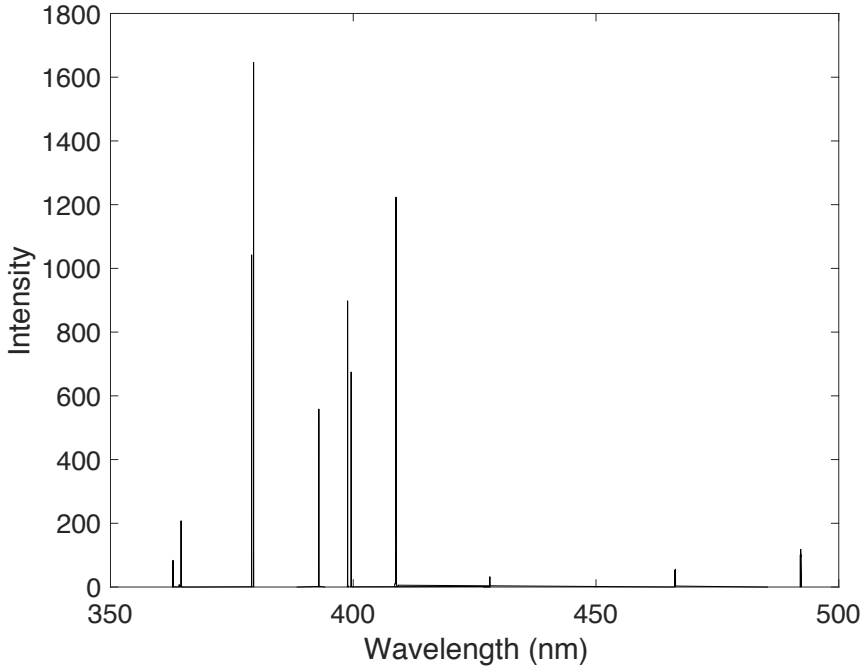

Fig. S1: Example composite spectrum of La ion and neutral emission, measured by the Shimadzu 9800 ICPOES.

Electron density

The electron density (N_e) was measured using the Stark effect, which is caused by the collisions of emitting species with electrons. The Stark effect is a phenomenon where ion-electron collisions cause measured emission peaks to broaden, with peak width correlating to electron density as:

$$N_e = C\Delta\lambda^{\frac{3}{2}} \text{x} 10^{19}$$

Where C is an experimentally determined constant (C = 35.8), and $\Delta\lambda$ is the full width at half maximum (FWHM) peak height of the emission line (constants and eq. (1) from (Boumans, 1987). The Stark effect is especially prevalent on Balmer series emission, so electron density was calculated using the FWHM of the H_β line at 468.1 nm, where the effect is most pronounced (Boumans, 1987; Aragón and Aguilera, 2008; Borkowska-Burnecka *et al.*, 2016).

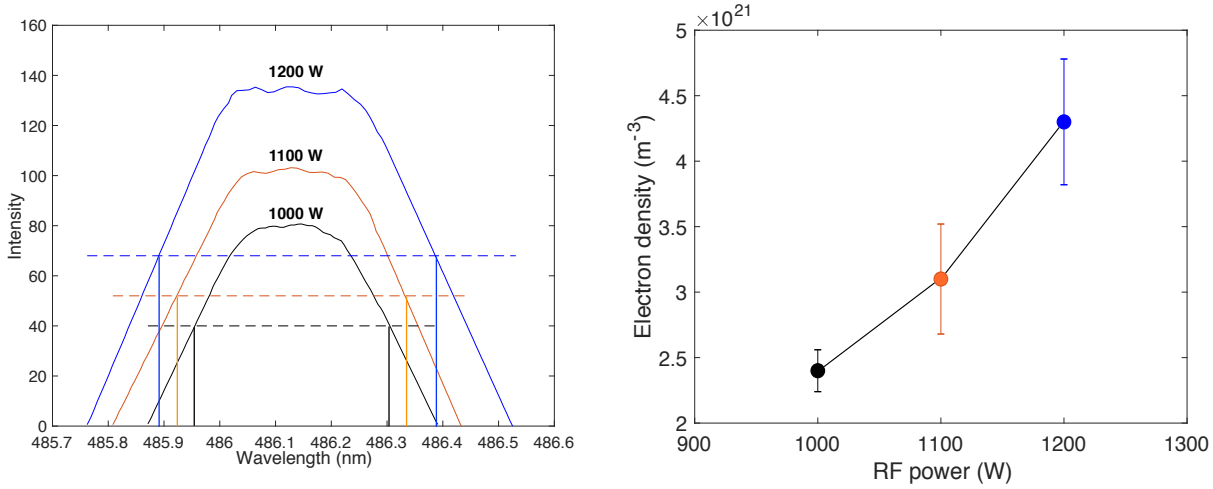

Fig. S2: (left) Measurement of H_β emission peak and the associated peak widening due to greater electron density at higher plasma RF power. (right) Electron density calculated from Stark broadening of H_β peak.

Peak width measurements show a progressive increase in electron density with increasing RF forward power, with N_e values ranging from $2.4\text{x}10^{21}$ m^{-3} at 1000 W to $4.3\text{x}10^{21}$ m^{-3} at 1200 W (Fig. 2) In atmospheric pressure RF plasmas, the total particle density approaches ~10^{24} m^{-3} with a typical Ar ion-neutral ratio of 10^{-3} at 7500 K (Niu and Houk, 1996). If we assume negligible electron contributions from 2^+ cations in this plasma, these values for electron density reflect the typical ionization state of a commercial Ar plasma.

Temperature

The emission intensity of a spectroscopic peak is dependent on the number of emitting species and by the temperature of the analyte. The Boltzmann method of temperature measurement was used to determine ion and neutral excitation temperatures in the plasma. The Boltzmann method uses the equation:

$$ln\left[\frac{\epsilon\lambda}{A_{jk}g_{jk}}\right] = \left[-\frac{1}{k_B T}\right]E + ln\left[\frac{hcN_o}{4\pi}\right]$$

where ε is peak emissivity, λ is the wavelength, A_{jk} is the emission efficiency, g_{jk} is the statistical weight of each transition. This takes the form of a line, y = mx+b. Plotting the highest energy level of a transition against $ln\left[\frac{\epsilon\lambda}{A_{jk}g_{jk}}\right]$ gives a linear trend, and the temperature of this system in units of K can be calculated from the slope as:

$$m = -\frac{1}{k_B T}$$

These plots give the temperature of the individual species, either an ion or neutral. In order to plot both ions and neutrals on the same plot, a correction is needed for the ion population for both the x and y axes. The correction applied to emission from the population of ions is:

$$X = \begin{cases} E_j\ (neutral) \\ E_J + E_{ion}\ (ion) \end{cases}$$

$$Y = \begin{cases} ln\left[\frac{\epsilon\lambda}{A_{jk}g_{jk}}\right]\ (neutral) \\ ln\left[\frac{\epsilon\lambda}{A_{jk}g_{jk}}\right] - ln\left[\frac{2\pi m_e k_B T}{h^3 N_e}\right]^{\frac{3}{2}}\ (ion) \end{cases}$$

The temperature found by Boltzmann plots of ion and neutral species is the excitation temperature, which is equal to the electron temperature (T_e) at atmospheric pressure. Thus, using the T_e and N_e values calculated above, we estimated the Saha ionization efficiency of the measured analyte.

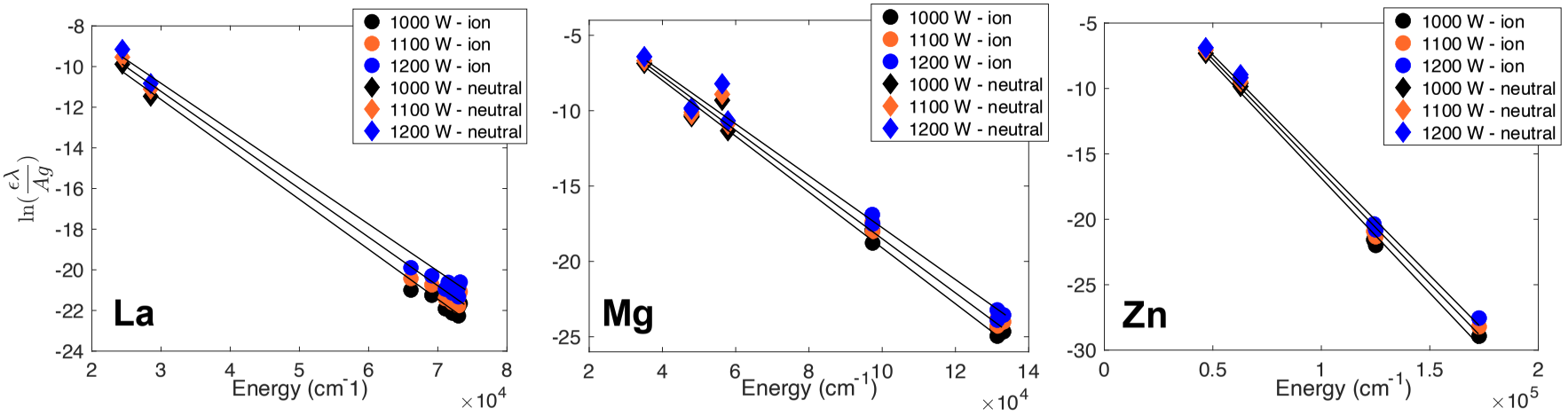

Fig. 3: Linear Boltzmann plots calculated for La, Mg, and Zn using measured emission from ion and neutral species.

Temperature (K)	1,000 W	1,100 W	1,200 W
Zn	8,000 ±240	8,200 ± 260	8,400 ± 270
Mg	8,100 ± 500	8,300 ± 580	8,400 ± 630
La	6,000 ± 1,100	6,100 ± 1,100	6,100 ± 1,200

Table 1: Excitation temperatures for each analyte measured via linear Boltzmann method.

Saha Ionization efficiency (%)	1,000 W	1,100 W	1,200 W
Zn	76 ± 6%	78 ± 11%	79 ± 9%
Mg	98 ± 9%	99 ± 15%	98 ± 15%
La	98 ± 19%	98 ± 22%	98 ± 2%

Table 2: Ionization efficiency estimated using the Saha equation, with values for T_e calculated from linear Boltzmann temperature measurements and N_e from Stark broadening of H_β lines.

Measurement of ion-neutral ratio

These Saha ionization efficiency values are compared to the measured ion-neutral ratio of emission lines from ion and neutral species in the plasma. The population densities of ions and neutrals are calculated from emission line intensities. The intensity of the emitting species is related to the population by:

$$N_o = \frac{\epsilon}{4\pi h\nu A_{jk} g_{jk}} e^{\frac{E}{k_B T}}$$

Using observed emission lines from ion and neutral species, average ionization efficiencies for the three element species are 70% Zn, 96% Mg, and 98% La. The measured ionization efficiencies are within 2-5% of the predicted Saha ionization efficiencies, despite the large measurement uncertainties. These measurements show that the Saha equation produces estimates of analyte ionization with high accuracy and give confidence that it is an appropriate predictor of the ionization capabilities of the experimental plasma.

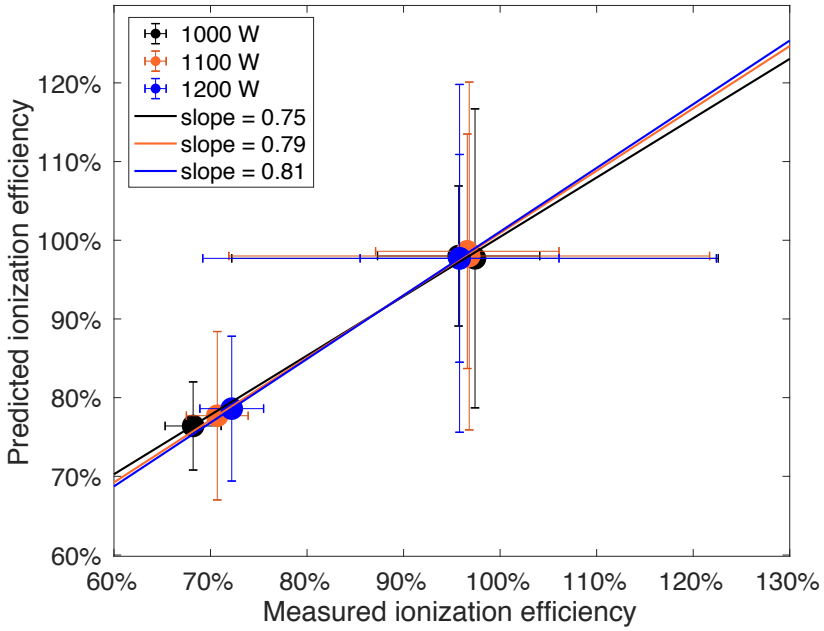

Fig. S4: Comparison of analyte ionization efficiency predicted by the Saha equation based on spectroscopic T_e and N_e measurements compared to measured ion-neutral ratios. Data points for Mg, La, and Zn.

Plasma interaction with injected sample

During laser ablation sampling, a distribution of particle sizes between 50-300 nm in diameter has been observed for commercial ultraviolet laser ablation systems with nano- to femtosecond pulse durations (Moná *et al.*, 2006). Consequently, the plasma needs to atomize particulates in this range. Here, we model the thermodynamics of the atomization process for this distribution of particle sizes. We also estimate the maximum mass loading the plasma can support and perform sample injection experiments with the plasma described in the main text.

a. Sample atomization

We calculate the total amount of energy needed to break all Si-O bonds in a silicate phase, assuming a spherical particle with uniform composition, conservatively modeled as pure SiO_2. This composition represents an upper limit of bond strengths in geologic materials (Si-O, 798 kJ/mol), as most ionic bonds (e.g. Fe-O, 409 kJ/mol) have lower bond strengths.

Ablated particles are injected into the plasma at high velocity and exposed to high gas temperatures for a transient amount of time. A gas flow rate of 200 SCCM (3.3 cm^3/s) through a sample injector tube with a 1 mm inner diameter achieves a gas velocity of >400 cm/s. If the end of the sample tube is positioned 1 cm from the plasma region, then a particle is exposed to the plasma environment for 2 ms. Based on this exposure time, we calculate the energy available to a silicate particle during transit:

$$E = \kappa t r T$$

Where κ is the thermal conductivity of silica (e.g., 1.3 W m^{-1} K^{-1}), t is the time the particle is exposed to the plasma (in s), r is the particle radius (in m), and T is the plasma gas temperature (in K). Using this equation, we find that a spherical particle 50 nm in diameter has ~$3x10^{-8}$ J imparted into the particle during exposure to a 500 K plasma, equivalent to the conditions measured for our He plasma at 19 W. Assuming a silicate particle with a mafic composition (Mg_2SiO_4, 140 g/mol), a 50 nm diameter particle contains $1.5x10^{-18}$ moles. With a dissociation energy for Si-O bonds of 798 kJ/mol, that particle requires $1.2x10^{-12}$ J to completely dissociate into atomic constituents. Thus, a single particle is exposed to four orders of magnitude more energy than is needed for complete dissociation.

According to this model, a plasma at 500 K is capable of atomizing ~31,000 particles with a 50 nm diameter, or ~1,100 particles with a diameter of 300 nm at any single point during standard operations (**Fig. S1**). However, gas expansion during injection from the sampler tube could accelerate the particles, leaving their exposure time lower than previously calculated. Thus, these estimates of mass load represent an upper bound. Consequently, the maximum mass load that the plasma can atomize is estimated at ~$2x10^{-9}$ g/s, comparable to the mass generated during laser ablation processing of a 40 μm diameter sample spot with a repetition rate of 10 Hz (assuming 50 nm depth incised per shot; (Pisonero and Gunther, 2008)).

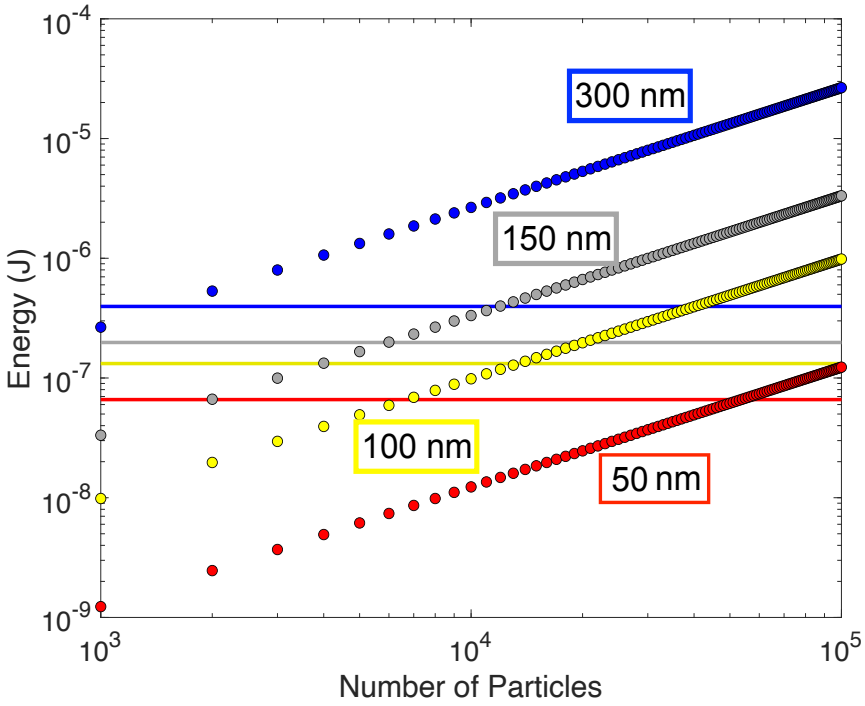

Fig. S5: Thermodynamic model estimating atomization efficiency of the 19 W He plasma (500 K gas temperature) described in the main text. This model shows the relationship between particle diameter and total number of particles that the plasma can atomize in a single point in time during standard operations. The solid lines represent the maximum amount of energy available to a single particle of a certain diameter, and curved lines show the total amount of energy necessary to atomize a population of particles of that same diameter.

b. Sample gas injection

A plasma was generated with 200 SCCM of He at 19 W of forward power. Different amounts of N_2 gas (representing analyte) were injected into this He plasma. Fig. 2 shows the change of ion current and electron density with increasing N_2 gas flow into the plasma. With increasing sample N_2 gas flow there is a decrease in the ion current and electron density of the plasma, showing a reduction in plasma performance with increasing sample mass load.

From the ideal gas law, a 10 SCCM gas flow rate is equivalent to 2.5×10^{-7} g/s of N_2 (**Fig. S2**), greater than the maximum mass loading the plasma can support (2×10^{-9} g/s, as described above).

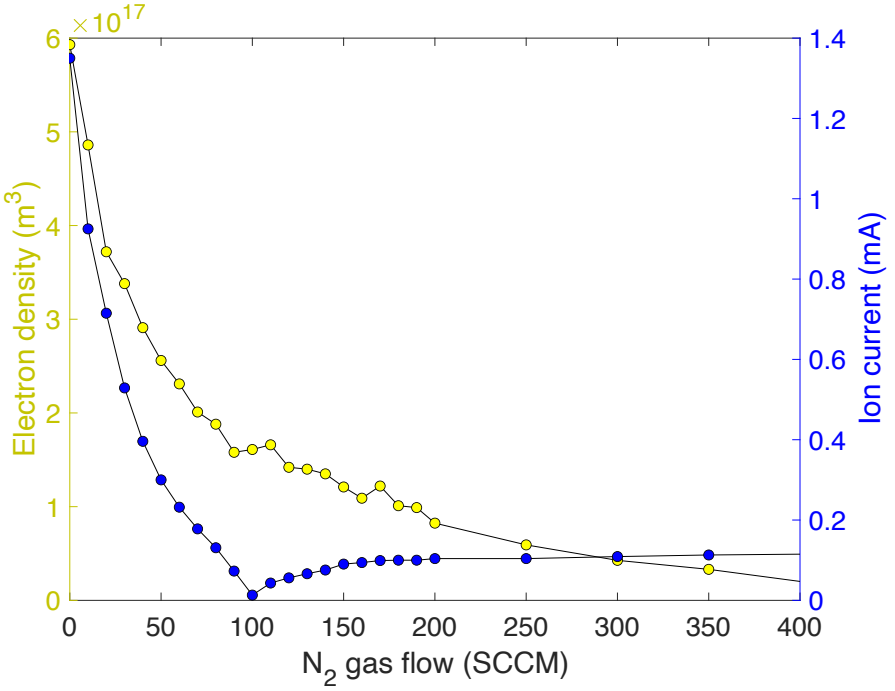

Fig. S6: Measurements of the electron density and ion current of the plasma as a function of introduced N_2 sample gas. Sample gas was mixed into a He plasma of 200 SCCM gas flow rate and 19 W of forward power.

References

Aragón, C. and Aguilera, J. A. (2008) 'Characterization of laser induced plasmas by optical emission spectroscopy : A review of experiments and methods', *Spectrochemica Acta part B*, 63, pp. 893–916. doi: 10.1016/j.sab.2008.05.010.

Borkowska-Burnecka, J. *et al.* (2016) 'Electron Density from Balmer Series Hydrogen Lines and Ionization Temperatures in Inductively Coupled Argon Plasma Supplied by Aerosol and Volatile Species', *International Journal of Spectroscopy*, 2016, pp. 11–13.

Boumans, P. W. J. M. (1987) *Inductively Coupled Plasma Emission Spectroscopy Part II: applications and fundamentals. Volume 2*. John Wiley & Sons, Inc.

Kramida, A., Ralchenko, Y. and Reader, J. (2018) *NIST Atomic Spectra Database (version 5.6.1)*, *National Institute of Standards and Technology, Gaithersburg, MD. DOI: https://doi.org/10.18434/T4W30F*.

Moná, V. *et al.* (2006) 'Quantitative analysis of Fe-based samples using ultraviolet nanosecond and femtosecond laser ablation-ICP-MS', *Journal of Analytical Atomic Spectrometry*, 21(11), pp. 1194–1201. doi: 10.1039/b606988f.

Niu, H. and Houk, R. S. (1996) 'Fundamental aspects of ion extraction in inductively coupled plasma mass spectrometry', *Spectrochemica Acta*, 51, pp. 779–815.

Pisonero, J. and Gunther, D. (2008) 'Femtosecond Laser Ablation Inductively Coupled Plasma Mass Spectrometry: Fundamentals and Capabilities for Depth Profiling Analysis', *Mass Spectrometry Reviews*, 27, pp. 609–623. doi: 10.1002/mas.